Deprotonation-Driven Phase Transformations in Terephthalic Acid Self-Assembly on Cu(100)

**S. Stepanow,[†] T. Strunskus,[‡] M. Lingenfelder,[†] A. Dmitriev,[†] H. Spillmann,[†] N. Lin,*,[†]
J. V. Barth,[§,||] Ch. Wöll,[‡] and K. Kern[†,§]**

*Max-Planck-Institut für Festkörperforschung, D-70569 Stuttgart, Germany, Lehrstuhl für Physikalische
Chemie I, Ruhr-Universität Bochum, D-44780 Bochum, Germany, Institut de Physique des Nanostructures,
Ecole Polytechnique Fédérale de Lausanne, CH-1015 Lausanne, Switzerland, and Advanced Materials and
Process Engineering Laboratory, Departments of Chemistry and Physics & Astronomy, University of
British Columbia, Vancouver, B.C. V6T 1Z4, Canada*

Received: July 21, 2004; In Final Form: October 8, 2004

Self-assembled terephthalic acid adlayers on a Cu(100) surface have been studied by X-ray photoelectron spectroscopy, near-edge X-ray absorption fine structure, and scanning tunneling microscopy in the temperature range 190−400 K under ultrahigh vacuum conditions. We observe three distinct well-ordered phases evolving with increasing temperature. The combined data analysis reveals that thermally activated deprotonation of molecular carboxyl groups is decisive in the irreversible transformation of the respective structures. Their self-assembly is mediated by changing intermolecular hydrogen bond configurations, whereby a flat adsorption geometry is retained.

Introduction

Hydrogen bonding is ubiquitous in the aufbau of biological systems and complex supramolecular structures.[1−4] Distinct three-dimensional architectures can be obtained using appropriately programmed molecular species, often designated as tectons. As the interaction is weak, it may be reversed. Accordingly, intrinsic error correction mechanisms are frequently operative in the self-assembly of hydrogen-bonded systems, leading ultimately to highly organized stable arrangements. In recent years, supramolecular engineering via hydrogen bonding at surfaces has attracted considerable interest and represents a promising route toward novel construction principles and materials with nanoscale control.[5−14] In particular, the careful choice of functional species providing geometrical (steric) and chemical complementarity allows for the tuning of two-dimensional molecular self-assembly.[5,8,11] On the other hand, substrate chemical activity and symmetry may strongly influence low-dimensional nanostructuring.[5,14,15] To guide the assembly of molecular architectures at surfaces, it is thus of great interest to elucidate the response of specific molecular moieties upon adsorption and their role in the evolution of supramolecular organizations.[10,11]

Benzoic acids proved to be versatile tectons for supramolecular engineering. A common motif in their organization is hydrogen bonding of the self-complementary carboxyl groups.[11,17,18] With the positioning of such species at copper surfaces, it turned out in the study of related systems that both flat-lying and upright-standing adsorption geometries are possible depending on the particular molecule used, substrate symmetry and temperature, and molecular coverage.[11,16] The observed bonding configurations reflect (partial) deprotonation of the carboxyl groups, different carboxylate coupling schemes to the substrate, and molecular interweaving hydrogen bonding.

Here, we report the results of combined X-ray photoelectron spectroscopy (XPS), near-edge X-ray absorption fine structure (NEXAFS), and scanning tunneling microscopy (STM) studies addressing the bonding and organization of terephthalic acid (TPA, 1,4-benzenedicarboxylic acid $C_6H_4(COOH)_2$, cf. Figure 1), adsorbed on a Cu(100) surface at different temperatures. We find that the carboxyl groups of the TPA molecules are (partially) deprotonated for temperatures exceeding 275 K. Three distinct phases are identified by STM in the temperature range 190−400 K. Their irreversible transformations with increasing temperature are associated with the deprotonation of carboxyl groups driving changes of intermolecular hydrogen bond configurations. XPS and NEXAFS measurements reveal the chemical nature of the molecules. The NEXAFS data show furthermore unambiguously that both the integral molecule and the terephthalate species adsorb in a flat-lying geometry.

Experimental Section

The X-ray photoelectron spectroscopy (XPS) and near-edge X-ray absorption fine structure (NEXAFS) measurements were carried out at the HE-SGM beamline at the Berlin synchrotron radiation facility BESSY II. The analysis chamber (base pressure better than $2 \cdot 10^{-10}$ mbar) was equipped with standard facilities for sample preparation, a quadrupole mass spectrometer, as well as a twin anode X-ray source and a CLAM2 energy analyzer. All NEXAFS spectra were recorded in the total electron yield (TEY) mode using a homemade electron detector based on a double channel plate (Galileo). For the energy calibration of the NEXAFS spectra, the photocurrent of a carbon-contaminated gold grid with a characteristic peak at 285 eV was recorded simultaneously with each spectrum. This grid was also used as a radiation flux monitor. For the NEXAFS experiments, the resolution was set to $\Delta E = 0.4$ eV at 300 eV. The C 1s NEXAFS raw data were normalized by a procedure consisting

---

* Author to whom correspondence should be addressed.
[†] Max-Planck-Institut für Festkörperforschung.
[‡] Ruhr-Universität Bochum.
[§] Ecole Polytechnique Fédérale de Lausanne.
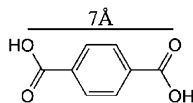[||] University of British Columbia.

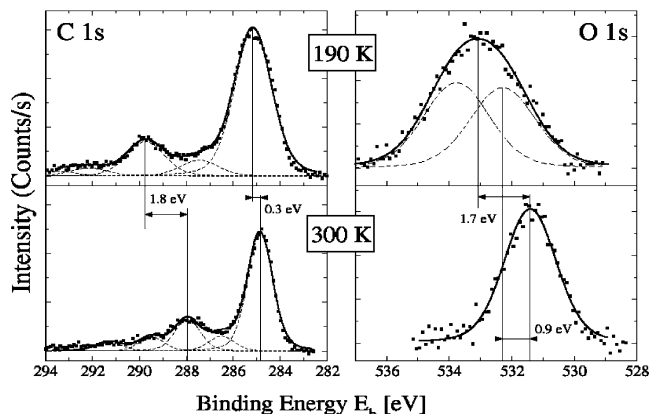**Figure 1.** Molecular structure and length of terephthalic acid.

Figure 2. XP spectra of the C 1s and O 1s for a TPA layer prepared at 190 K (upper graphs) and following annealing at 400 K for 30 min (measured at room temperature, lower graphs). The data (squares) have been fitted by a set of one to six Voigt-type curves. The fwhm parameters for the Voigt-curves in the O 1s region are 2.47 and 1.98 eV for the substrate at low and room temperature, respectively. Peak positions are marked by vertical lines. The deconvolution of the broad low-temperature oxygen peak reflects the two chemically different carboxyl oxygen, while the sharpened peak appearing upon annealing is associated with equivalent oxygen in the diterephthalate species. The larger low-energy peaks in C 1s are from aromatic carbon and the smaller high-energy peaks are attributed to carbon of carboxyl and carboxylate side groups, respectively.

of several steps. First, the spectrum recorded for the clean substrate was multiplied with a correction factor to yield equal intensities in the energy range 272−278 eV and then subtracted. The resulting data were then normalized to the photon flux by division through a spectrum obtained for a freshly sputtered gold wafer. Finally, the spectra were normalized to yield an edge jump (difference intensity between 275 and 325 eV) of one. The XP data for the carbon 1s and oxygen 1s peak were acquired with a beam energy of 400 and 650 eV, respectively. The pass energy of the analyzer was set to 50 eV. For quantitative analysis, a complete set of XP spectra was acquired in addition with the Al Kα -radiation of the laboratory source with a pass energy set to 100 eV. All spectra have been referenced to the Cu $3p_{3/2}$ line at 75.1 eV. The STM data were obtained using a home-built beetle-type instrument incorporated in a UHV system with a base pressure of ∼3 × 10^{-10} mbar. The STM measurements were performed in the constant current mode using a tungsten tip with substrate temperatures in the 230−300 K range.

The Cu(100) sample was prepared by several cycles of Ar$^+$ sputtering and subsequent annealing at 800 K. TPA (99+%, Sigma-Aldrich Chemie GmbH) in powder form was deposited by organic molecular beam epitaxy (OMBE) from a Knudsen-cell type evaporator, held at 440 K during deposition.

Results and Discussion

XPS. Temperature-dependent XPS measurements were carried out to characterize and identify the chemical states of carbon and oxygen. In Figure 2, the XP data for a TPA adlayer on the Cu(100) surface is presented. The upper curves show the XP spectra of TPA deposited and measured on a substrate held at

190 K, whereas the graphs below show the spectra measured at room temperature after the same sample was annealed at 400 K for 30 min. For deconvolution and determination of the exact peak positions, the data were fitted after background subtraction by one to six Voigt-type curves for the oxygen and carbon 1s peaks, respectively, with an asymmetry parameter very close to 1. Within a given spectrum, the full width at half-maximum (fwhm) parameter was fixed for the fit curves.

For TPA deposited at low temperature in the O 1s region, a broad peak exists at 533.1 eV (Figure 2, upper-right), which can be decomposed into two almost equal-height contributions with peak positions at 532.3 and 533.8 eV. In accordance with earlier observations,[17,19−23] these two peaks are assigned to oxygen in the carbonyl and hydroxyl group, respectively. Upon annealing, a marked sharpening of the O 1s peak occurs, which is now centered at 531.4 eV (Figure 2, bottom-right). The single symmetric and narrow peak is associated with two chemically identical oxygen atoms in the carboxylate moieties, clearly distinguishable from the broader peak in the low-temperature spectrum. The binding energy of the oxygen 1s electron in the carboxylate moieties is by 0.9 eV lower than in the carbonyl group.[23]

Two well-separated peaks can be identified in the C 1s region for the low-temperature phase, at 285.2 and 289.7 eV (Figure 2, upper-left). The large peak at low energy is assigned to the six carbon atoms in the aromatic ring and the high-energy peak to the two carbon atoms in the carboxyl groups.[20,22] The origin of the intensity around 287 eV is not known. It is not found in the multilayer C 1s core level spectrum of TPA (not shown here). Possible explanations are final state effects or a partial decomposition of the TPA molecules at defects on the copper surface. The small peak at about 292 eV is attributed to a $\pi-\pi^*$ shake-up transition of the aromatic system. Upon annealing, the position of the main carbon peak remains almost constant at 284.9 eV, whereas the smaller high-energy signal vanishes and instead a peak shifted to a lower binding energy at 288 eV emerges, which is attributed to carbon in carboxylate groups.[20,22] The ratio of the total intensity of the oxygen 1s and carbon 1s spectra does not change upon annealing, which signifies that apart from the carboxyl deprotonation the TPA molecules remain intact (the overall intensity reduction is attributed to thermal desorption of a fractional second molecular layer existing at low temperature).

The XPS data of both oxygen and carbon strongly suggest the following scenario: at 190 K TPA molecules exist as integral species on the substrate, whereas upon the annealing carboxyl groups are fully deprotonated and the diterephthalate is formed. Deprotonation of carboxyl groups upon adsorption at Cu surfaces was similarly reported for other benzoic acid species.[10,11,16,17,24] There is general agreement that the hydrogen formed in this process is thermally desorbed. We will demonstrate below that the deprotonation plays a decisive role in the two-dimensional molecular self-assembly.

NEXAFS. NEXAFS spectra recorded for the different TPA adlayers are displayed in Figure 3. Following deposition of TPA at 190 K, several pronounced π^*-resonances are clearly discernible. The π^*-resonance at 284.6 eV and the shoulder at 285.3 eV are assigned to transitions related to the carbon atoms of the aromatic ring, whereas the prominent peak at 288.1 eV, the shoulder at 288.8 eV, and the small resonance at 289.9 eV are assigned to transitions related to the carboxyl carbons. The remaining transitions at 292.8 eV, 296.4 eV, and the broad hump at 301 eV reflect σ^*- transitions. Both the π^*-resonances of the phenyl carbons and of the carboxyl carbons show a
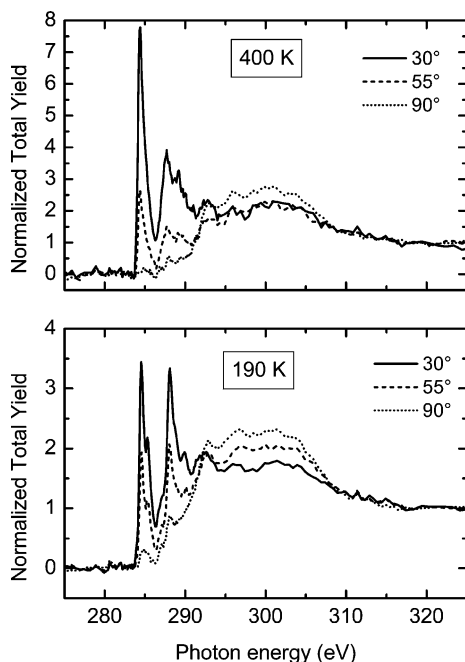
Figure 3. NEXAFS spectra recorded at the C *K*-edge for a TPA monolayer prepared at 190 K (lower graph) and after annealing at 400 K for 30 min (measured at room temperature, upper graph). Solid and dashed lines indicate spectra obtained at different angles of incidence of the synchrotron light (90° means normal incidence to the Cu(100) surface).

Figure 4. (a−c) STM images of the three molecular phases of TPA observed at different temperatures. Arrows indicate the [011] direction of the Cu(001) surface. (a) One of the four domains of the α-phase imaged at 230 K. (b) β-phase imaged at room temperature. (c) γ-phase obtained by 400 K annealing imaged at room temperature. (d−f) Tentative models for the three phases shown in a−c. Hydrogen bonds are represented by dashed lines. Bonding motifs are highlighted by oxygen and hydrogen atoms marked as "O" and "H" for one molecule in each model. Aromatic ring hydrogen not involved in hydrogen-bond formation is omitted for clarity. The unit cells of the three phases, $\begin{bmatrix} 3 & 0 \\ 1 & 3 \end{bmatrix}$, $\begin{bmatrix} 2 & -2 \\ 4 & 5 \end{bmatrix}$, and (3 × 3), are drawn. Open circles represent copper surface atoms. The high-symmetry [001] and [010] directions of the substrate are indicated.

pronounced dichroism with almost completely vanishing intensity for normal photon incidence (90°). For perfectly flat-lying molecules, the intensity of the π^*-resonances should vanish completely at normal photon incidence. The small intensity remaining at 90° in the experimental spectra can be interpreted in terms of a uniform tilt of the plane of all molecules about 5° relative to the surface. However, it is more likely that the vast majority of the molecules is indeed adsorbed in a perfectly flat geometry and merely a small number of molecules deviates significantly from a flat adsorption geometry. These latter molecules can be adsorbed at defects or step edges or even in a second layer. This can occur especially at 190 K where molecular mobility is low and second layer thermal desorption does not occur.

Upon warming to 400 K and measuring the sample again at 300 K, the dichroism of the π^*-resonances is even more pronounced (cf. Figure 3, upper graph). This indicates that the molecules remain in a flat-lying geometry on the Cu(100) surface. In the benzene ring region, the first π^*-resonance at 284.6 eV has increased in intensity and the second resonance at 285.3 eV is not resolved anymore, whereas in the carboxyl carbon region now two π^*-resonances at 287.8 and 289.2 eV of almost equal intensity prevail. The latter two resonances seem to be shifted to lower energy upon warming to 400 K, which is in good agreement with the shift of the carboxyl peak in the C 1s core level data. The marked change in the carboxyl carbon region in the NEXAFS spectrum thus further supports the XPS data, notably confirming complete deprotonation of the carboxyl groups upon annealing.

STM. Three distinct topologies were observed when TPA molecules were adsorbed at substrate temperatures in the 230−400 K range. In Figure 4a−c, we show representative STM images of the three phases. Besides step decoration, the molecules form ordered structures on the terraces. All phase transformations are irreversible when the sample is cooled to low temperatures.
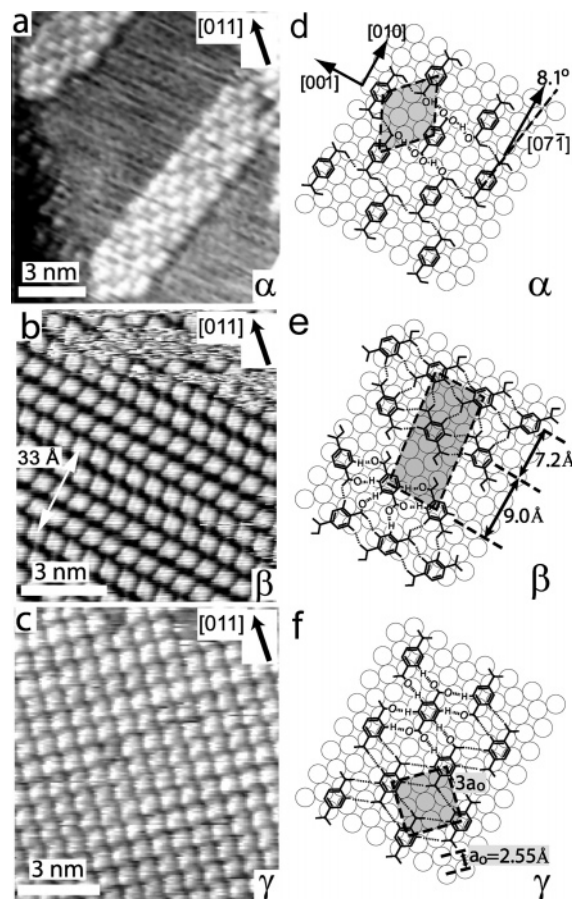
An ordered low-temperature phase (cf. Figure 4a), henceforth denoted as α-phase, was observed upon TPA deposition at 230 K. The existence of molecular ribbons implies that there is appreciable mobility and anisotropic interactions under these conditions. The molecules are free to transport on the surface until they are incorporated into the ribbons, whose formation also implies edge mobility; otherwise, irregular or fractal islands in a diffusion-limited process would be expected.[5,14,25] Defining the orientation of a ribbon as its principal axis, four different oriented principal axes are identified. Considering the fourfold symmetry of the substrate, there are two distinguishable island directions forming an angle of about ±8 degrees with the substrate high-symmetry directions [010] or [001]. Each island consists of several (at least two) rows of molecules running in the principal direction. Size and shape of the molecular features in the STM images agree well with the size of the TPA backbone, which is ∼7 Å length (cf. Figure 1). This confirms the flat-lying adsorption geometry concluded from the NEXAFS data. Within a row, the distance between the adjacent molecules is about 12.8 Å, whereas adjacent rows have a spacing of about

Deprotonation-Driven Phase Transformations

J. Phys. Chem. B, Vol. 108, No. 50, 2004 **19395**

4.1 Å. The long axis of the molecular features in the STM images is parallel to the principal direction of the islands.

At a temperature of ∼275 K, a first structural transformation occurs. The α-phase is replaced by close-packed molecular domains. This new molecular phase (denoted as β-phase) is depicted in Figure 4b. The β-phase can either be obtained upon annealing the α-phase or—as for the experiment of Figure 4b—directly by molecular deposition on the substrate held at 275−300 K. A detailed inspection reveals that the β-phase domains consist of paired molecular rows following either [010] or [001] direction of the substrate. TPA molecules now exhibit a rhomb shape with the diagonal aligning along [011] or [01$\bar{1}$]. Shape and size of the two differently oriented molecules are identical. The periodicity along the molecular rows amounts to about 7 Å. Molecules within a paired row are oriented in a complementary way. The row-to-row distance between TPA within a paired row is about 7 Å, whereas the interpair distance is about 9 Å. This is reflected in the more pronounced dark stripes between the paired rows. The alternative arrangement of the paired rows produces a wavelike structure with a periodicity of about 33 Å perpendicular to the row directions.

The β-phase is further transformed into a third layer structure, the γ-phase, upon 400 K annealing. It is depicted in Figure 4c and can be obtained similarly with the β-phase either via sample annealing or directly by molecular deposition with the substrate at 400 K. It is stable up to a temperature of 500 K. The molecules in this phase can form large regular domains extended over entire terraces with an almost perfect long-range ordering. The structure is built up from a square-shaped unit cell with a dimension of 7.6 Å, which matches 3 times the surface lattice constant (2.55 Å). The long axis of the oval molecular features in the STM image (Figure 4c) is aligned either in the [010] or [001] direction, reflecting the existence of two rotational domains.

Taking into account the XPS data, the structural transitions observed by STM are ascribed to the deprotonation of the carboxyl groups of the TPA molecules. Respective tentative models are shown in Figure 4d−f. The molecular geometry of TPA used in the modeling is taken from diffraction studies of organic crystals.[18] In the models, the molecules are adsorbed flat, with their aromatic rings parallel to the surface, in accordance with the NEXAFS data. From the absence of long-range height modulations in the STM topography, we conclude distinct molecular adsorption sites for all phases. For the modeling, the aromatic ring is positioned at the fourfold hollow site, since this site has often been observed for other aromatic molecules on metal surfaces.[26−28] Hydrogen bonds stabilize all three phases; the respective bond lengths at surfaces can relax from the ideal hydrogen bond lengths observed in three-dimensional arrangements because of the influence of substrate atomic lattice and metal surface electrons.

For the α-phase, the data analysis suggests that TPA molecular rows are coupled by hydrogen bonds between the oxygen of the carbonyl groups and the hydrogen of the hydroxyl group in the cis position in contrast to the well-known 1-D carboxyl chain motif in bulk TPA[18] (cf. the model shown in Figure 4d). Each TPA is engaged in four hydrogen bonds with its neighbors, that is, the number of bonds per molecule is 2. The O···H−O distance in the hydrogen bonds is estimated to be 3.0 Å, larger than the bulk TPA distance of 2.69 Å reported in ref 18. The molecules are aligned along [07$\bar{1}$] or equivalent directions, forming an angle of 8.1° with respect to substrate high-symmetry direction, as indicated in Figure 4d. This alignment is defined by two factors: the positioning of the

aromatic ring and an appropriate intermolecular distance for hydrogen-bond formation. The molecular rows similarly follow the [07$\bar{1}$] direction, agreeing well with the observed angle between the two observed reflection domains. The unit cell of this phase can be assigned as

$$\begin{bmatrix} 3 & 0 \\ 1 & 3 \end{bmatrix}$$

respecting to the (100) substrate. Because of the fourfold symmetry of the substrate, the model explains naturally the occurrence of four domain orientations. Since the packing of the ribbons accounts for an enantiomorphic structure, two domains are mirror-symmetric configurations, respectively (cf. detailed discussion in ref 5).

The model of the β-phase is depicted in Figure 4e. It consists of paired molecular rows running along the [001] direction. The molecular axis—as inferred from the rhombohedral shape—either aligns with the [011] or the [01$\bar{1}$] direction. We propose that each TPA molecule has at least one deprotonated carboxyl group; whether the second one is deprotonated or not is not obvious from our data (cf. detailed discussion below). The pairing suggests two types of hydrogen bonds, both involving carboxylate coupling to aromatic ring hydrogen. The respective O···H−C distance is 3.0 (3.1) Å for the intrarow (inter-row) case, slightly shorter than a value found for a similar motif in a 3-D structure (>3.3 Å).[29] Each TPA forms six hydrogen bonds with its neighbors; the number of bonds per molecule is thus 3. The inter-row distance is 7.2 Å within and 9.0 Å between the paired rows, consistent with the measured values (as shown in Figure 4e). We suggest that the inter-row hydrogen bonds are only present within paired rows but not between them (cf. detailed discussion below). The unit cell of this structure is

$$\begin{bmatrix} 2 & \text{-}2 \\ 4 & 5 \end{bmatrix}$$

The model of the γ-phase is depicted in Figure 4f. In this case, both carboxyl groups of TPA molecule are deprotonated (cf. XPS analysis). TPA molecules arrange in a (3 × 3) unit cell with respect to the substrate (hightlighted by the gray square in Figure 4f), with the molecular long axis aligned in the [010] direction. Similar to the case in the β-phase, the arrangement of the molecules suggests hydrogen bonds between carboxylate oxygen and aromatic ring hydrogen, with an O···H−C length of 3.4 Å, which is comparable to similar bonds in the solid state, while remaining at the lower limit.[29] Every molecule is now engaged in eight hydrogen bonds of the same type to its neighbors. Thus, the number of bonds per molecules has further increased to four.

Upon deposition of TPA molecules on the substrate held at room temperature, we observed the coexistence of β and γ-phases. To directly investigate the temporal evolution of the molecular structures, a series of consecutive STM images were taken at the same area on the surface. The data, shown in Figure 5, were acquired at 4-min intervals (Figure 5a−c) with the exception of the last one (Figure 5d), taken 1 h after the first image (Figure 5a). An arrow marks a vacancy representing a reference feature. At first glance, it is conspicuous that the molecules in the β-phase are brighter than the features in the γ-phase, which is believed to correspond to a higher conductivity of the β-phase molecules. In this series of images, the area of the γ-phase grows with time at the expense of the β-phase, as seen, for example, in figure 5a−c at the left part of the γ-phase. We have never observed the reverse process. In this particular
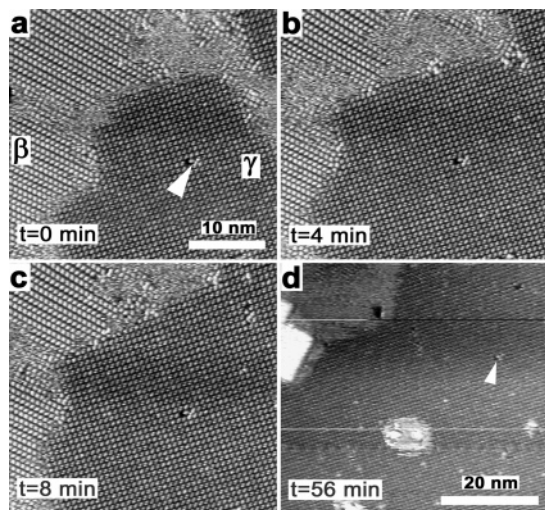
Figure 5. Series of consecutive STM images recorded at the same surface area at room temperature following TPA deposition at 300 K. The images were acquired at 4-min intervals (a−c) and (d) 1 hour after a. An arrow marks a defect representing a reference position. The area covered by the γ-phase grows with time at the expense of the β-phase.

example (Figure 5a−d), the influence of the tip seems irrelevant since image 5d was taken 45 min later without any scanning after image 5c. However, the tip influence cannot be excluded in general: we always observed pure β-phase even 4 h after the initial molecular deposition, but after a first scan in such a region parts of the island turned into the γ-phase. Nevertheless, after an annealing at 400 K for 5 min, the β-phase totally disappeared and only the γ-phase was observed.

Experimentally, it is nontrivial to correlate the β-phase to the XPS data because of its metastable nature; thus, we cannot determine conclusively the deprotonation state of the β-phase carboxyl groups unambiguously. Nevertheless, the observed room-temperature transition from β- to γ-phase is interpreted as follows: Presumably in the β-phase, TPA is only partially (i.e., one carboxyl group) deprotonated, and between TPA molecules in neighboring paired rows hydrogen bonds are prevented. Under the 400 K annealing or tip influence, the second carboxyl groups are deprotonated and tansformation to γ-phase may occur. The second possibility is that both carboxyl groups of the molecules are already deprotonated in the β-phase but the gap between the paired rows is too wide for hydrogen-bond formation. In the 275−300 K temperature range, this phase is thermally metastable and an external disturbance (thermal energy or tip-induced influence) may trigger the transition to the energetically favored γ-phase.

Benzoic acid adsorption on copper surfaces was similarly studied for related systems.[10,11,15−17,24,30,31] Quite generally, the carboxyl groups deprotonate (partially) upon adsorption and exceeding system-specific threshold temperatures, and highly ordered phases evolve. For example, on Cu(100) benzoic acid deprotonates between 120 and 170 K whereas the deprotonation of trimesic acid sets in at about 290 K.[11,17] Interestingly, a molecular reorientation occurs with several of these systems. Evidence exists that in the structural transition of TMA layers on Cu(100) partially deprotonated molecules change to an upright-standing adsorption geometry to switch back to flat adsorption upon when the tri-trimesate species is formed.[11,24] By contrast, for trimellitic acid deposition on the Cu(100) substrate held at 400 K, a highly ordered phase evolves with just one deprotonated carboxyl group, where the aromatic ring is strongly tilted away from the surface plane.[30] In addition, a coverage-dependent phase transformation was reported for

benzoic acid and TPA on Cu(110), where the orientation changes from flat-lying to upright with carboxylate anchoring at surface atoms at high coverage.[16,17] Moreover, in a series of experiments, the formation of 2D Cu−carboxylate coordination compounds incorporating copper adatoms and flat-lying molecules interferes.[17,24,31] At the present stage, no general rules can be derived describing the evolution of benzoic acid arrangements on Cu surfaces. While (sequential) carboxylate formation is a common feature, the delicate balance of intermolecular H-bonding, carboxylate formation with surface or adatoms, and steric matching decides on the specific structure formed.

Conclusions

The bonding and self-assembly of TPA on a Cu(100) surface has been studied by STM, XPS, and NEXAFS in the temperature range 190−400 K. The molecules organize in highly ordered domains comprising well-defined structural motifs. We identified three phases with distinct topologies. Deprotonation of the carboxyl moieties of the molecule underlies the respective irreversible phase transformations occurring with increasing temperature. The supramolecular ordering is rationalized by the interplay between molecule−substrate interaction and intermolecular hydrogen bonding. With the present system, the structural changes with increasing temperature reflect carboxylate formation with TPA retaining a flat bonding geometry, which drives changing 2D hydrogen bond configurations.

References and Notes

(1) Lehn, J.-M. *Supramolecular Chemistry: Concepts and Perspectives;* VCH: Weinheim, Germany, 1995.

(2) Philp, D.; Stoddart, J. F. *Angew. Chem., Int. Ed. Engl.* **1996**, *35*, 1154.

(3) Jeffrey, G. A.; Saenger, W. *Hydrogen bonding in biological systems;* Springer: Berlin, 1991.

(4) Prins, L. J.; Reinhoudt, D. N.; Timmerman, P. *Angew. Chem., Int. Ed.* **2001**, *40*, 2382.

(5) Barth, J. V.; Weckesser, J.; Cai, C.; Günter, P.; Bürgi, L.; Jeandupeux, O.; Kern, K. *Angew. Chem., Int. Ed.* **2000**, *39*, 1230.

(6) Kawai, T.; Tanaka, H.; Nakagawa, T. *Surf. Sci.* **1997**, *386*, 124.

(7) Weckesser, J.; De Vita, A.; Barth, J. V.; Cai, C.; Kern, K. *Phys. Rev. Lett.* **2001**, *87*, 096101.

(8) Yokoyama, T.; Yokoyama, S.; Kamikado, T.; Okuno, Y.; Mashiko, S. *Nature* **2001**, *413*, 619.

(9) Böhringer, M.; Morgenstern, K.; Schneider, W.-D.; Berndt, R.; Mauri, F.; De Vita, A.; Car, R. *Phys. Rev. Lett.* **1999**, *83*, 324.

(10) Chen, Q.; Frankel, D. J.; Richardson, N. *J. Chem. Phys.* **2002**, *116*, 460.

(11) Dmitriev, A.; Lin, N.; Weckesser, J.; Barth, J. V.; Kern, K. *J. Phys. Chem. B* **2002**, *106*, 6907.

(12) Chen, Q.; Richardson, N. *Nat. Mater.* **2003**, *2*, 324.

(13) Theobald, J. A.; Oxtoby, N. S.; Phillips, M. A.; Champness, N. R.; Beton, P. H. *Nature* **2003**, *424*, 1029.

(14) Barth, J. V.; Weckesser, J.; Trimarchi, G.; Vladimirova, M.; De Vita, A.; Cai, C.; Brune, H.; Günter, P.; Kern, K. *J. Am. Chem. Soc.* **2002**, *124*, 7991.

(15) Perry, C. C.; Haq, S.; Frederick, B. G.; Richardson, N. V. *Surf. Sci.* **1998**, *409*, 512.

(16) Martin, D. S.; Cole, R. J.; Haq, S. *Phys. Rev. B* **2002**, *66*, 155427.

(17) Chen, Q.; Perry, C. C.; Frederick, B. G.; Murray, P. W.; Haq, S.; Richardson, N. V. *Surf. Sci.* **2000**, *446*, 63.

(18) Sledz, M.; Janczak, J.; Kubiak, R. *J. Mol. Struct.* **2001**, *595*, 77.

(19) Dubois, L. H.; Zegarski, B.; Nuzzo, R. *Langmuir* **1986**, *2*, 412.

(20) Han, S. W.; Joo, S. W.; Ha, T. H.; Kim, Y.; Kim, K. *J. Phys. Chem. B* **2000**, *104*, 11989.

(21) Parker, B.; Immaraporn, B.; Gellman, A. J. *Langmuir* **2001**, *17*, 6638.

(22) Wühn, M.; Weckesser, J.; Wöll, C. *Langmuir* **2001**, *17*, 7605.

(23) Lindberg, B.; Berndtsson, A.; Nilsson, R.; Nyholm, R. *Acta Chem. Scand. A* **1978**, *32*, 353.

(24) Lin, N.; Dmitriev, A.; Weckesser, J.; Barth, J. V.; Kern, K. *Angew. Chem., Int. Ed.* **2002**, *41*, 4779.

(25) Witten, T. A.; Sander, L. M. *Phys. Rev. B* **1983**, *27*, 5686.

Deprotonation-Driven Phase Transformations

J. Phys. Chem. B, Vol. 108, No. 50, 2004 **19397**

(26) Hallmark, V. M.; Chiang, S.; Meinhardt, K. P.; Hafner, K. *Phys. Rev. Lett.* **1993**, *70*, 3740.

(27) Chiang, S. *Chem. Rev.* **1997**, *97*, 1083.

(28) Lee, A. F.; Wilson, K.; Lambert, R. M.; Goldoni, A.; Baraldi, A.; Paolucci, G. *J. Phys. Chem. B* **2000**, *104*, 11729.

(29) Steiner, T.; Saenger, W. *Acta Crystallogr., Sect. B* **1992**, *48*, 819.

(30) Dmitriev, A.; Spillmann, H.; Lin, N.; Barth, J. V.; Kern, K. *Angew. Chem., Int. Ed.* **2003**, *41*, 2670.

(31) Barth J. V.; Weckesser, J.; Lin, N.; Dmitriev, A.; Kern, K. *Appl. Phys. A* **2003**, *76*, 645.